Inversion for anisotropy from non-double-couple components of moment tensors

Václav Vavryčuk

Geophysical Institute, Academy of Sciences of the Czech Republic, Prague, Czech Republic

Received 3 December 2003; revised 30 April 2004; accepted 13 May 2004; published 10 July 2004.

[1] An inversion method for retrieving seismic anisotropy from non-double-couple components of seismic moment tensors is presented. The method requires a set of highly accurate moment tensors of earthquakes that occurred in a homogeneous anisotropic focal area on differently oriented faults. In contrast to standard methods retrieving anisotropy from travel times or from shear wave splitting, which yield an overall anisotropy averaged along a whole ray path, the presented method yields a local value of anisotropy just in the focal area. The method is robust, being able to retrieve the orientation as well as strength of anisotropy even for low anisotropy symmetries as for orthorhombic symmetry. The method can utilize the moment tensors constrained to have zero trace, but using unconstrained moment tensors is advantageous. The method is applied to retrieving anisotropy in the Tonga subduction zone using moment tensors of deep-focus earthquakes reported in the Harvard centroid moment tensor catalog. The inversion is complemented by tests on synthetic data to assess its stability and the accuracy of the results. The inversion indicates that the subduction zone is anisotropic with orthorhombic symmetry. The orientation of the intra-slab anisotropy is defined by axes (azimuth/dip) $a_1 = 320°/54°$, $a_2 = 121°/38°$, and $a_3 = 223°/81°$. The errors in the azimuth and dip are about 5°. The first and second axes lie along the downdip motion of the slab and along the normal to the slab, respectively. The strength of the *P*, *S*1, and *S*2 anisotropy is of 7.3 ± 1.5%, 13.4 ± 2.5%, and 12.6 ± 3.5%, respectively. The errors of anisotropy strength are only rough estimates, which reflect random but not systematic errors in the moment tensors used in the inversion. The values for anisotropy strength in the slab are remarkably higher than those observed in the surrounding mantle. The symmetry axes of anisotropy coincide with the principal stress directions in the slab. This manifests a primary impact of stress on anisotropy formation. The retrieved anisotropy in the slab can serve as an additional constraint on its structure and mineralogical composition. *INDEX TERMS:* 7260 Seismology: Theory and modeling; 7215 Seismology: Earthquake parameters; 7218 Seismology: Lithosphere and upper mantle; 8164 Tectonophysics: Stresses—crust and lithosphere; *KEYWORDS:* seismic anisotropy, moment tensors, earthquakes, subduction zones

Citation: Vavryčuk, V. (2004), Inversion for anisotropy from non-double-couple components of moment tensors, *J. Geophys. Res.*, *109*, B07306, doi:10.1029/2003JB002926.

1. Introduction

[2] The non-double-couple (non-DC) components in moment tensors of earthquakes are frequently observed and are attributed to various causes [*Frohlich*, 1994; *Julian et al.*, 1998; *Miller et al.*, 1998]. They can be spurious, being a product of unmodeled path effects [*Kuge and Lay*, 1994; *Šílený and Vavryčuk*, 2000, 2002], of a poor station coverage, or of an oversimplification of the source process in a moment tensor inversion [*Sipkin*, 1986; *Kuge and Kawakatsu*, 1992, 1993]. But they can also be real, reflecting specific properties of a source or of a focal area. The true non-DC components can be caused by landslides [*Hasegawa and Kanamori*, 1987], inflation or deflation of magma chambers in volcanic areas [*Mori and McKee*, 1987], or tensile faulting owing to high pore fluid pressure in geothermal or volcanic areas [*Vavryčuk*, 2001, 2002]. The non-DC components have also been reported for rock bursts in mines [*Rudajev and Šílený*, 1985; *Feignier and Young*, 1992].

[3] Another mechanism causing non-DC components of moment tensors is faulting in an anisotropic medium [*Kawasaki and Tanimoto*, 1981]. This mechanism could occur quite frequently because anisotropy seems to be a pervasive property of geological structures [*Babuška and Cara*, 1991]. Usually, anisotropy is not very strong, but it can still generate non-negligible non-DC components in moment tensors of earthquakes. The non-DC components can thus contain information on anisotropy in a focal area, and, in principle, non-DC components could be used to determine the anisotropy.

0148-0227/04/2003JB002926$09.00

[4] In this paper, I propose an inversion for anisotropy of a focal area from non-DC components of moment tensors. I present a mathematical description of the inversion and demonstrate its power on synthetic tests. Finally, I discuss applications to deep-focus earthquakes in the Tonga-Kermadec subduction zone, the most active zone in the world, which offers a large data set of moment tensors of deep earthquakes. The deep earthquakes are particularly suitable for this study because (1) the moment tensors of deep earthquakes are determined with a higher accuracy than those of shallow earthquakes; (2) deep earthquakes often display non-DC components; and (3) deep earthquakes occur in subducting slabs, which are assumed to be anisotropic [*Fukao*, 1984; *Kendall and Thomson*, 1993; *Hiramatsu et al.*, 1997; *McNamara et al.*, 2002]. It is speculated that anisotropy in the slab is caused by an alignment of metastable olivine and its polymorphs wadsleyte and ringwoodite or the ilmenite form of pyroxene [*Anderson*, 1987; *Mainprice et al.*, 2000]. The intra-slab anisotropy can also be induced by strain due to large stresses generated when a rigid slab encounters the 670 km discontinuity [*Wookey et al.*, 2002]. Therefore it is worth applying the proposed inversion to earthquakes in a slab to decide whether the intra-slab anisotropy is really significant and appreciably contributes to the non-DC components of deep earthquakes or whether the non-DC components have only other causes, such as numerical errors due to unmodeled path effects and complex shear faulting at faults or subfaults with different orientations [*Miller et al.*, 1998; *Estabrook*, 1999; *Tibi et al.*, 2003].

2. Theory

2.1. Moment Tensors of Earthquakes in Anisotropic Media

[5] A seismic moment tensor $\mathbf{M}$ describing shear faulting in an isotropic medium is expressed as [*Aki and Richards*, 2002, equation 3.22]

$$M_{kl} = \mu u S(\nu_k n_l + \nu_l n_k). \tag{1}$$

Equation (1) is the common double-couple representation of the earthquake source, which can be inverted for the fault normal $\mathbf{n}$, the slip direction $\boldsymbol{\nu}$, and the product μuS of the slip u, the shear modulus μ, and the fault area S. Obviously, μ, u, and S cannot be separated from one another.

[6] Contrary to equation (1), the seismic moment tensor $\mathbf{M}$ of an earthquake in anisotropic media is more complicated, being expressed as [*Aki and Richards*, 2002, equation 3.19]

$$M_{kl} = uSc_{ijkl}\nu_i n_j, \tag{2}$$

where c_{ijkl} are the elastic parameters of the medium surrounding the fault and the Einstein summation convention over repeated subscripts is applied. This moment tensor comprises the double-couple (DC) and also the isotropic (ISO) and the compensated linear vector dipole (CLVD) components [*Knopoff and Randall*, 1970; *Jost and Hermann*, 1989]. The non-DC components (ISO and CLVD) can be nonzero even for shear earthquakes [*Kawasaki and Tanimoto*, 1981]. In general, the higher the strength of anisotropy, the higher are the values of the non-DC components that can be expected.

[7] Next, the percentage of the ISO and CLVD components will be calculated according to *Vavryčuk* [2001, 2002]:

$$\mathrm{ISO} = \frac{1}{3}\frac{\mathrm{Trace}(\mathbf{M})}{|M_{|\max|}|}(100\%) \tag{3}$$

$$\mathrm{CLVD} = -2\frac{M^*_{|\min|}}{|M^*_{|\max|}|}(100\% - |\mathrm{ISO}|) \tag{4}$$

$$\mathrm{DC} = 100\% - |\mathrm{ISO}| - |\mathrm{CLVD}|, \tag{5}$$

where $\mathrm{Trace}(\mathbf{M})$ denotes the trace of $\mathbf{M}$ and $M_{|\max|}$ denotes the eigenvalue of $\mathbf{M}$ which has the maximum absolute value. Tensor $\mathbf{M}^*$ denotes the deviatoric part of the moment tensor $\mathbf{M}$,

$$\mathbf{M}^* = \mathbf{M} - \frac{\mathbf{I}}{3}\mathrm{Trace}(\mathbf{M}), \tag{6}$$

where $\mathbf{I}$ is the 3×3 identity matrix. Quantities $M^*_{|\max|}$ and $M^*_{|\min|}$ are the eigenvalues of $\mathbf{M}^*$ with the maximum and minimum absolute values, respectively.

2.2. Inversion for Anisotropy

[8] Equation (2) can be used for the inversion for elastic parameters of a medium in the focal area. If we know the moment tensors of N earthquakes that occurred in an anisotropic focal area with constant elastic parameters, equation (2) represents a system of $6N$ equations for $5N$ unknown parameters describing unit vectors $\mathbf{n}$ and $\boldsymbol{\nu}$ and product uS for each earthquake and for m elastic parameters describing anisotropy in the focal area. If the earthquakes under study are due to shear faulting ($\boldsymbol{\nu} \perp \mathbf{n}$), the number of unknown parameters is reduced from $5N$ to $4N$. The extent and quality of the moment tensor data set limit the number of anisotropic parameters m which can be inverted for. A general triclinic anisotropy is described by 21 elastic parameters c_{ijkl}. However, two of them must always be fixed to overcome the problem of the coupling between elastic parameters c_{ijkl}, slip u, and fault area S and the problem of special geometry in shear faulting. For example, for isotropy, which is described by two parameters, no information on the medium can be gained from the moment tensors of shear earthquakes, but one parameter (e.g., the ratio of the Lamé coefficients λ/μ) can be determined from the moment tensors of tensile earthquakes [*Vavryčuk*, 2001]. Hence one can invert at most for 19 elastic parameters describing anisotropy. This task requires at least moment tensors of 10 shear earthquakes. However, because of noise in data it is more plausible to invert for anisotropy of higher symmetry and use a much larger number of moment tensors. For example, inverting for orthorhombic symmetry reduces the number of unknown parameters from 21 to 12 (three angles define the orientation of the principal axes, and nine elastic parameters define orthorhombic anisotropy). Inverting for transverse isotropy (TI) reduces the number

of unknown parameters from 21 to 7 parameters (two angles define the direction of the symmetry axis, and five parameters define TI).

2.3. Misfit Function

[9] For the purpose of the inversion, equation (2) can be modified as follows:

$$\mathbf{m} = uS\mathbf{C}\mathbf{d}, \tag{7}$$

where $\mathbf{C}$ is the 6×6 matrix of the elastic parameters in the two-index Voigt notation [*Musgrave*, 1970, equation 3.13.4] and $\mathbf{m}$ and $\mathbf{d}$ are the six vectors defined as

$$\mathbf{m} = (M_{11}, M_{22}, M_{33}, M_{23}, M_{13}, M_{12})^T \tag{8}$$

$$\mathbf{d} = (n_1\nu_1, n_2\nu_2, n_3\nu_3, n_2\nu_3 + n_3\nu_2, n_1\nu_3 + n_3\nu_1, n_1\nu_2 + n_2\nu_1)^T. \tag{9}$$

The left-hand side of equation (7) represents observations; the right-hand side of equation (7) is unknown, being a product of unknown elastic parameters $\mathbf{C}$ and unknown geometry of faulting $\mathbf{d}$. The elastic parameters $\mathbf{C}$ are common for all earthquakes, while vector $\mathbf{d}$ is specific for each earthquake. Therefore it is convenient to separate them and to invert only for elastic parameters $\mathbf{C}$,

$$\mathbf{d} = u^{-1}S^{-1}\mathbf{C}^{-1}\mathbf{m}. \tag{10}$$

The six vector $\mathbf{d}$ is closely related to the symmetric dyadic tensor $\mathbf{D} = \mathbf{n}\boldsymbol{\nu} + \boldsymbol{\nu}\mathbf{n}$

$$\mathbf{D} = \begin{bmatrix} 2n_1\nu_1 & n_1\nu_2 + n_2\nu_1 & n_1\nu_3 + n_3\nu_1 \\ n_1\nu_2 + n_2\nu_1 & 2n_2\nu_2 & n_2\nu_3 + n_3\nu_2 \\ n_1\nu_3 + n_3\nu_1 & n_2\nu_3 + n_3\nu_2 & 2n_3\nu_3 \end{bmatrix}, \tag{11}$$

to which the following conditions should apply:

$$\mathrm{Trace}(\mathbf{D}) = n_1\nu_1 + n_2\nu_2 + n_3\nu_3 = 0 \tag{12}$$

$$\mathrm{Det}(\mathbf{D}) = 0. \tag{13}$$

Equation (12) is a condition for shear faulting; equation (13) follows from the fact that a dyadic product of two vectors has one zero eigenvalue. Conditions (12) and (13) apply to moment tensors of each earthquake and can be employed when inverting for elastic parameters $\mathbf{C}$. In the inversion we search such elastic parameters $\mathbf{C}$ that satisfy

$$\sum_{j=1}^{N} \left[\left| \mathrm{Trace}\left(\mathbf{D}^j\right) \right| + \left| \mathrm{Det}\left(\mathbf{D}^j\right) \right| \right] = \min, \tag{14}$$

where

$$\mathbf{D} = \begin{bmatrix} 2d_1 & d_6 & d_5 \\ d_6 & 2d_2 & d_4 \\ d_5 & d_4 & 2d_3 \end{bmatrix}. \tag{15}$$

Superscript j means that the quantity is evaluated for the jth earthquake, and N stands for the total number of moment tensors inverted. Since the inversion cannot yield absolute values of elastic parameters $\mathbf{C}$ (two elastic parameters must always be fixed), we can equally invert either for elastic parameters $\mathbf{C}$ (if we fix two elastic parameters) or for the density-normalized elastic parameters $\mathbf{A} = \mathbf{C}/\rho$, where ρ is the density of the medium (if we fix two normalized elastic parameters). Using equations (10), (14), and (15), we can invert for elastic parameters $\mathbf{C}$ or for the normalized parameters $\mathbf{A}$ without the necessity to determine fault normal $\mathbf{n}$ and slip direction $\boldsymbol{\nu}$ for each earthquake.

2.4. Inversion of Moment Tensors With Zero Trace

[10] The moment tensors are often determined under the assumption that their trace is zero:

$$\mathrm{Trace}(\mathbf{M}) = M_{11} + M_{22} + M_{33} = 0. \tag{16}$$

This condition is used because it is justified for shear earthquakes in isotropic media and stabilizes moment tensor inversions. However, if the focal area is anisotropic or the earthquake is not shear [*Miller et al.*, 1998; *Vavryčuk*, 2001], such inversion yields distorted results and has undesirable consequences. First, the number of independent parameters of the moment tensor of each earthquake is reduced from 6 to 5. This reduces the number of independent equations in the inversion for anisotropy from $6N$ to $5N$, where N is the total number of moment tensors used. This implies that when inverting for anisotropy, we should employ a higher number of zero-trace moment tensors than the moment tensors calculated without any constraint. Second, the inversion procedure for anisotropy must be modified to be applicable also to the zero-trace moment tensors.

[11] Assume that only the deviatoric part $\mathbf{M}^*$ of moment tensors $\mathbf{M}$ can be utilized. Using the six-vector notation

$$\mathbf{m}^* = \left(M_{11}^*, M_{22}^*, M_{33}^*, M_{23}^*, M_{13}^*, M_{12}^*\right)^T \tag{17}$$

and inserting equation (7) into equation (6), we obtain

$$\mathbf{m}^* = uS\left[\mathbf{C}\mathbf{d} - \frac{\mathbf{i}}{3}\mathrm{Trace}(\mathbf{C}\mathbf{d})\right] = uS\mathbf{B}\mathbf{d}, \tag{18}$$

where quantity $\mathbf{i}$ is the unit six vector, $\mathbf{i} = (1,1,1,1,1,1)^T$, and the components of matrix $\mathbf{B}$ read

$$B_{IJ} = C_{IJ} - \frac{1}{3}(C_{1J} + C_{2J} + C_{3J}) \tag{19a}$$

for $I = 1, 2, 3$, $J = 1, \ldots, 6$ and

$$B_{IJ} = C_{IJ} \tag{19b}$$

for $I = 4, 5, 6$, $J = 1, \ldots, 6$. Consequently,

$$\mathbf{d} = u^{-1}S^{-1}\mathbf{B}^{-1}\mathbf{m}^*. \tag{20}$$

This equation together with conditions (14) and (15) defines the inversion of zero-trace moment tensors.

3. Application to the Tonga Subduction Zone

3.1. Data

[12] The proposed inversion is applied to moment tensors of deep earthquakes in the Tonga-Kermadec subduction zone. This zone displays the most intense deep seismicity in the world, which is caused by the subduction of the Pacific Plate under the Australian Plate. The rate of the subduction is 10.5 cm/yr [*DeMets et al.*, 1990; *Gripp and Gordon*, 1990]. The direction of motion is N300°E, being perpendicular to the strike of the slab and of the Tonga-Kermadec Trench. The geometry of the slab is complicated, in particular, at the northern end of the deep part of the slab [*Hamburger and Isacks*, 1987; *Giardini*, 1992]. The slab subducts steeply with a dip of about 60°. The subducting slab displays high P and S velocity anomalies of several percent [*Zhou*, 1990a; *Deal et al.*, 1999; *Koper et al.*, 1999] because the slab is about 800°C cooler than the surrounding mantle [*Anderson*, 1987].

[13] I use moment tensors of earthquakes available in the Harvard centroid moment tensor (CMT) catalog [*Dziewonski et al.*, 2001, 2003]. This global earthquake catalog seems best in the completeness and accuracy of its solutions [*Kagan*, 2003]. Since the inversion used in this paper is data demanding, I do not use data from other less comprehensive catalogs such as the United States Geological Survey (USGS) catalog [*Sipkin et al.*, 2002] or the catalog of the Earthquake Research Institute in Tokyo [*Kawakatsu*, 1995]. Neither do I combine data from different catalogs to avoid mixing moment tensors that are of different quality and that are determined using different methods. All the catalogs mentioned produce the zero-trace moment tensors and use isotropic Green functions in the inversion. The use of isotropic Green functions is justified by the fact that the inversion employs large wavelengths, which are sensitive not to local variations of anisotropy in the mantle but rather to an overall mantle anisotropy which is small, probably not exceeding 2% [*Savage*, 1999]. The justifiability of the zero-trace constraint is disputable for shallow earthquakes but seems to be reasonably satisfied for deep earthquakes, as was proven by several authors [*Kawakatsu*, 1991, 1996; *Hara et al.*, 1995].

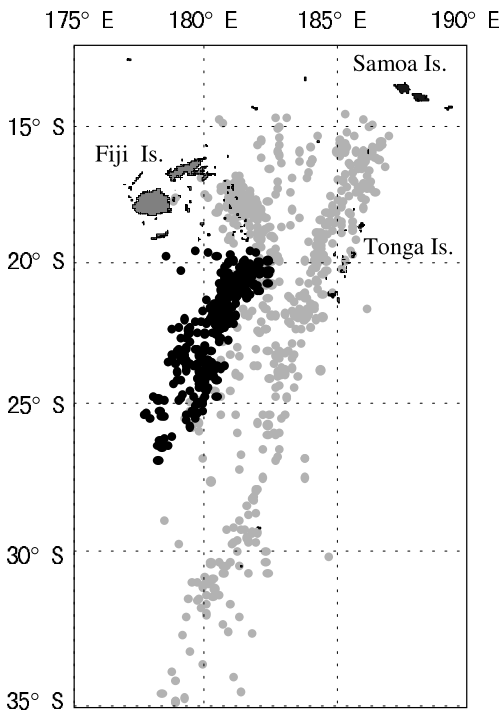

Figure 1. Epicenters of earthquakes in the Tonga subduction zone. Black circles mark the deep-focus earthquakes under study (depth >500 km, southern cluster); gray circles mark the other earthquakes in the region (depth >100 km).

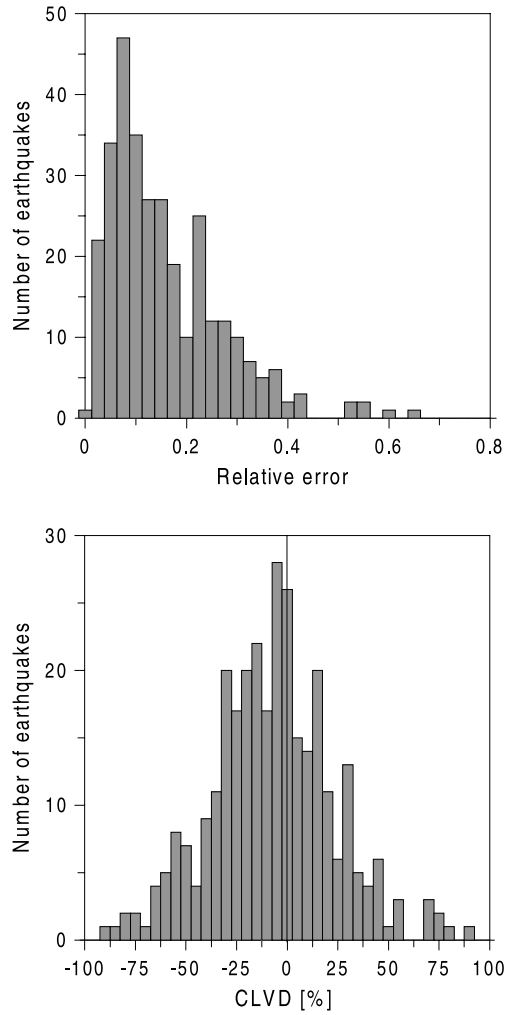

Figure 2. Histograms of (top) relative errors and (bottom) CLVD of moment tensors for the Tonga earthquakes in the southern cluster.

[14] I selected earthquakes with magnitudes $M_w > 5$ that occurred in the period 1980–2002 and were located at latitudes 19.5°–27°S, longitudes 177°E–177°W, and depths between 500 and 700 km (see Figure 1). The southern part of the Tonga active zone was selected to avoid complexities in earthquake parameters due to the sharp bending of the subducted slab in the north [*Hamburger and Isacks*, 1987; *Giardini and Woodhouse*, 1984; *Giardini*, 1992; *Northard et al.*, 1996]. The selected moment tensors are of different

Table 1. Data Sets of Moment Tensors[a]

Data Set	Moment Tensors	Relative Error, %	Mean DC, %	Mean CLVD, %	Mean |CLVD|, %
A	70	0.08	84.7	−9.4	15.2
B	82	0.09	84.4	−9.2	15.6
C	95	0.10	85.2	−8.7	14.8
D	105	0.11	85.3	−8.5	14.7
E	113	0.12	85.2	−7.2	14.8
Original[b]	310	0.65	75.7	−7.3	24.3

[a]DC and CLVD percentages were calculated using equations (3)–(5).
[b]Original moment tensors have no constraints on the CLVD and on the relative error.

accuracy and display a different amount of the CLVD component (see Figure 2). In order to analyze the most reliable moment tensors, I further selected from the total number of 310 moment tensors only those with an absolute value of CLVD less than 40% because an extremely high value of CLVD indicates either an anomalous mechanism (e.g., the mechanism which changed during rupture) or difficulties in the moment tensor inversion. Furthermore, the moment tensors were selected to have a relative error less than a threshold value. The relative error is defined as the ratio of the largest singular value of the standard error **E** reported in the catalog and of the largest singular value of the moment tensor **M**. To assess the influence of errors present in moment tensors on the inversion results, threshold values 0.08, 0.09, 0.10, 0.11, and 0.12 were set up. The threshold value could not be smaller than 0.08 because the number of moment tensors satisfying such a strict constraint was too low for a reliable inversion. Also, the threshold value could not be higher than 0.12 because the inversion started to be unstable, probably because of the rather high noise in the data. Hence five different data sets of different extent and quality were analyzed, and the results were compared. The data sets comprised moment tensors of 70, 82, 95, 105, and 113 earthquakes (see Table 1).

3.2. Slab Geometry and Stress in the Slab

[15] The foci of selected earthquakes cluster in a belt oriented in accord with the subducting slab. Interpolating the foci by a plane, we infer that the strike of the slab is N210°E, and the dip is 50° (see Table 2). The error of the strike/dip is about 5°/10°. The strike N210°E corresponds to the strike of the Tonga-Kermadec Trench. The dip of 50° is slightly less than the 60° determined for shallower depths. Variations in the dip of the slab with depth have also been reported by other authors [*Zhou*, 1990b; *Northard et al.*, 1996; *Karato et al.*, 2001]. Note that the geometry of the northern part of the slab (Figure 1) is remarkably different [*Hamburger and Isacks*, 1987; *Giardini*, 1992].

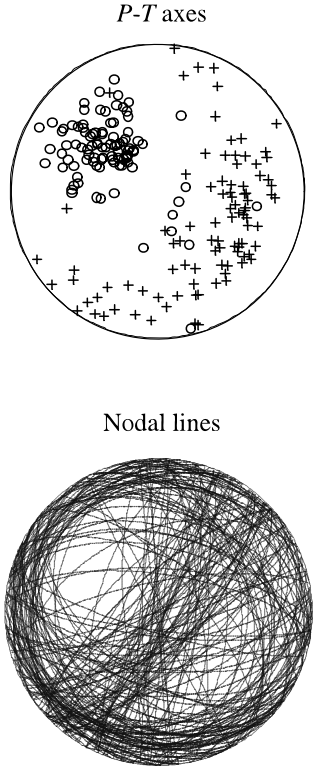

Figure 3. (top) *P*-*T* axes and (bottom) nodal lines for the focal mechanisms of data set C. The *P* axes are marked by circles; the *T* axes are marked by plus signs. Lower hemisphere equal-area projection is used.

[16] Stress in the focal area is inferred from focal mechanisms by applying the Gephart and Forsyth inversion method [*Gephart and Forsyth*, 1984; *Michael*, 1987; *Gephart*, 1990; *Lund and Slunga*, 1999] to the selected earthquakes. The majority of the studied mechanisms are normal or reverse with subvertical and subhorizontal nodal lines (Figure 3). The *P* axes form a concentrated cluster (with some exceptions), but the *T* axes are more scattered. In the inversion the stress tensor is sought over a grid by minimizing the sum of deviations between the predicted shear traction directions and the observed slips at the faults. The method is able to retrieve three angles defining the directions of the three principal stress axes σ_1, σ_2, and σ_3 and shape ratio R, which bounds the size of the principal stresses: $R = (\sigma_1 - \sigma_2)/(\sigma_1 - \sigma_3)$. The inversion for the optimum stress was performed using a 5° grid in searching through the principal stress directions. The values of the resultant stress are summarized in Table 2; the misfit

Table 2. Slab Orientation and Stress in the Slab[a]

Data Set	Moment Tensors	Relative Error, %	Slab Strike/Dip, deg.	Slab Normal Azimuth/Dip, deg.	Sigma 1 Azimuth/Dip, deg.	Sigma 2 Azimuth/Dip, deg.	Sigma 3 Azimuth/Dip, deg.	Shape Ratio
A	70	0.08	210/54	120/54	310/50	122/40	217/86	0.74
B	82	0.09	210/54	120/54	315/45	121/46	218/83	0.72
C	95	0.10	209/51	119/51	310/45	123/45	216/86	0.70
D	105	0.11	209/50	119/50	310/50	115/41	214/82	0.70
E	113	0.12	209/43	119/43	310/50	115/41	214/82	0.70

[a]Azimuth is measured from the north, and dip is measured from the vertical.

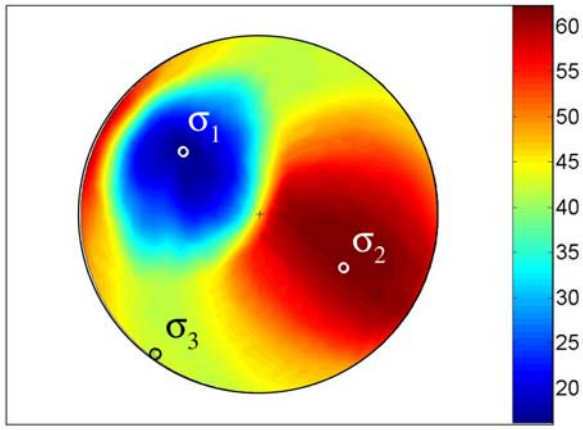

Figure 4. Inversion for stress using moment tensors of data set C. The plot shows the misfit function for the stress axis σ_1, defined as an average deviation (in degrees) between predicted shear traction directions and observed slips at the faults. The misfit function is displayed in the lower hemisphere equal-area projection. The optimum directions of the principal stresses are marked by circles.

function for data set C is shown in Figure 4. The stress found is consistent with results obtained by other authors [*Isacks and Molnar*, 1971; *Frohlich*, 1989; *Zhou*, 1990b; *Guest et al.*, 2004]. The maximum compression and tension axes are parallel to the subducting slab: The compression axis follows the subduction flow, and the tension axis is mostly horizontal and parallel to the trench. The intermediate stress axis is perpendicular to the slab. The downdip compression in the deep parts of slabs is frequently observed and is interpreted as resistance to subduction due to resisting forces at the tip of the slab [*Zhou*, 1990b].

3.3. Non-DC Components

[17] The presence of the non-DC components in moment tensors and their accuracy are essential for the anisotropy inversion. Several authors studied the accuracy of the DC and non-DC (CLVD) components reported in the CMT and other catalogs [*Helffrich*, 1997; *Frohlich and Davis*, 1999; *Kagan*, 2003]. They showed that the DC components are, in general, much better constrained than the CLVD components. The errors in the CLVD components are frequently high and can easily be exemplified by correlating the CLVD of the earthquakes reported jointly in the CMT and USGS catalogs. Surprisingly, this correlation is almost zero when all jointly reported earthquakes are considered. However, the correlation increases for deep earthquakes. For example, data set E contains 56 jointly reported moment tensors, and the correlation coefficient between the CLVD is 0.303. The average correlation between the full moment tensors is 0.935. The correlation coefficient between moment tensors $\mathbf{M}^{(1)}$ and $\mathbf{M}^{(2)}$ is defined as

$$c = \frac{M_{ij}^{(1)} M_{ij}^{(2)}}{\sqrt{M_{kl}^{(1)} M_{kl}^{(1)}}\sqrt{M_{mn}^{(2)} M_{mn}^{(2)}}}. \qquad (21)$$

Figure 5 indicates that the non-DC components in the selected moment tensors are real but are appreciably affected by noise. The noise is probably generated by unmodeled path effects due to a complex velocity structure.

[18] Figure 6 and Table 1 show the CLVD and DC components in the studied data sets. The CLVD takes positive as well as negative values, but the negative values slightly prevail. With a decreasing accuracy of moment tensors in a data set this imbalance tends to vanish. No dependence of the CLVD on the depth of earthquake foci is observed. The CLVD is slightly reduced for earthquakes with magnitudes higher than 6.

3.4. Inversion Algorithm

[19] I assume anisotropy in the slab of orthorhombic symmetry, which is typical for mantle minerals such as olivine, wadsleyite, or ringwoodite [*Mainprice et al.*, 2000]. Special cases of orthorhombic symmetry are cubic symmetry (typical for garnet) or transverse isotropy, which could be generated, for example, by laminations in the slab. More general anisotropy is not considered because of limitations of input data. Orthorhombic symmetry is

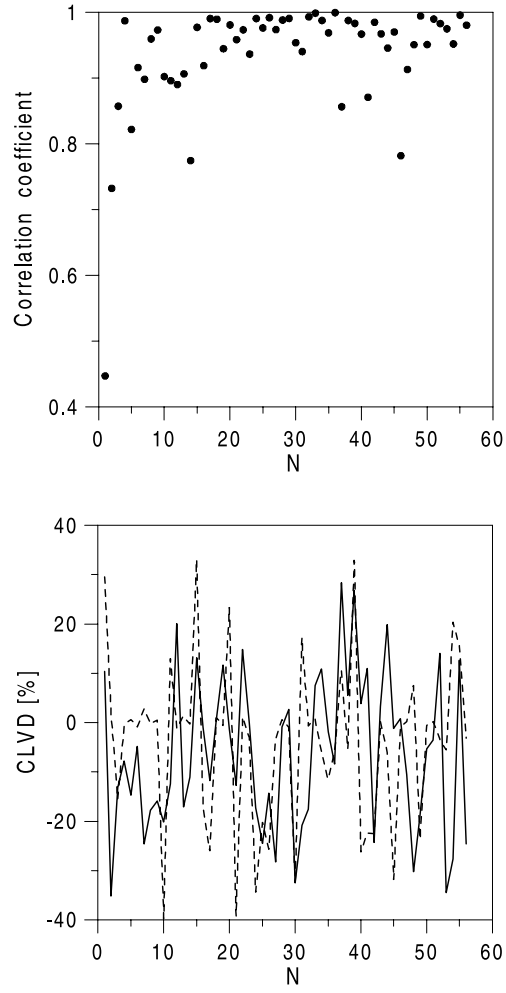

Figure 5. (top) Correlation coefficient between moment tensors and (bottom) the CLVD components in moment tensors for 56 earthquakes jointly reported in the CMT and USGS catalogs. *N* denotes the sequential number of the earthquake sorted by origin time. The dashed/solid line shows the USGS/CMT data.

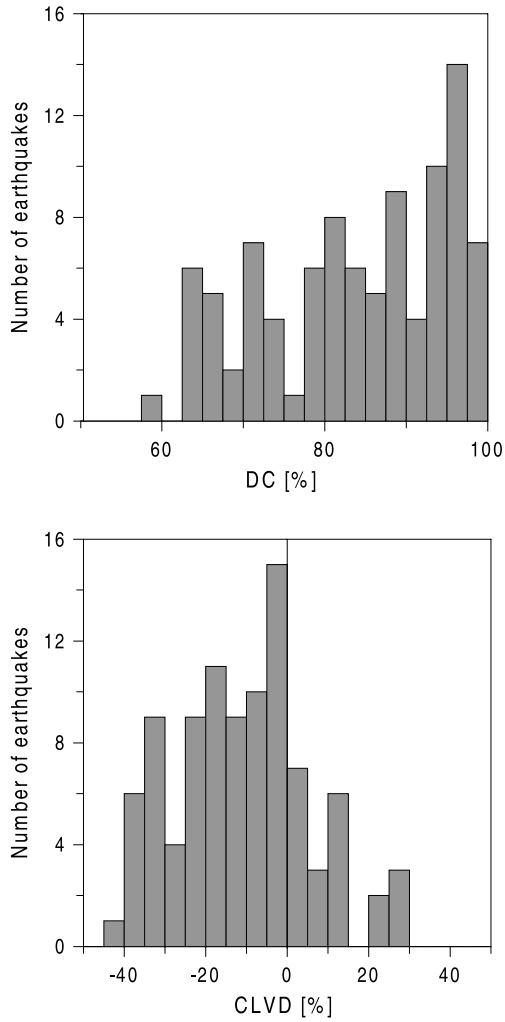

Figure 6. Histograms of (top) DC and (bottom) CLVD components in the moment tensors of data set C. The ISO components are identically zero because the moment tensors are constrained to have zero trace.

described by 12 parameters: by nine density-normalized elastic parameters A_{11}, A_{22}, A_{33}, A_{44}, A_{55}, A_{66}, A_{12}, A_{13}, and A_{23} and by three angles defining the orientation of the system of the symmetry axes. Since two elastic parameters must be fixed, we can invert for 10 parameters. To calculate the misfit function (14), formula (20) designed for the moment tensors with zero trace was used. The minimum of the misfit function is determined by combining a simple grid search with algorithms of the MATLAB Optimization Toolbox [*Branch and Grace*, 1996] designed for solving constrained nonlinear optimization problems [*Powell*, 1978; *Gill et al.*, 1991]. The constrained nonlinear optimization is used for seeking elastic parameters; the grid search is used for finding the optimum orientation of anisotropy axes. Hence to each orientation of the system of symmetry axes I applied the nonlinear optimization search for optimum values of elastic parameters and for evaluating the corresponding misfit function. The global optimum solution was found at the global minimum of the misfit function sought over a grid of all directions of symmetry axes. The constrained rather than unconstrained optimization for seeking elastic parameters was used to avoid false minima related to unrealistic anisotropy. In order to stabilize the results of the inversion and to obtain statistically more relevant results, I do not present parameters of the only optimum solution, but I have averaged the parameters over the 25 best solutions.

3.5. Synthetic Tests

[20] Synthetic tests were performed to demonstrate that the inversion method is capable of retrieving anisotropy from a data set similar to that under study. I assumed an orthorhombic anisotropy in the focal area with the elastic parameters given in Table 3. The symmetry axes were inclined by angles (azimuth/dip) a_1 = 313°/50°, a_2 = 125°/40°, and a_3 = 220°/86°. The azimuth is measured from the north and the dip from the vertical. For this medium, synthetic moment tensors were generated in the following way. The DC components of 70 moment tensors grouped with data set A were used. Then synthetic non-DC components caused by the prescribed anisotropy were generated, and the complete synthetic moment tensors were constructed. Then random noise was superimposed on the moment tensors to simulate the moment tensors observed. Noise is supposed to simulate spurious non-DC components caused by a poor station coverage or complex velocity structure used in the moment tensor inversion and true non-DC components caused by other effects than anisotropy (e.g., complex source mechanism).

[21] Three levels of random noise were used to assess the stability of the inversion: The first level was comparable with the noise in the observed moment tensors; the second level was slightly higher; and the third level was more than two times higher than the observed noise (see Figure 7). The data sets obtained were inverted for anisotropy. The elastic parameters A_{33} and A_{44} were fixed at true values. The values of the other parameters were sought within the intervals given in Table 3. The orientation of the system of symmetry axes was searched over a sphere in a grid with a step of 10°.

[22] Table 4 summarizes the results of the inversion. The optimum values presented (i.e., the orientations of the symmetry axes and strength of anisotropy) were calculated as medians of the 25 best solutions found by the inversion. The optimum values of anisotropy strength are presented together with their standard deviations. The most stable parameters recovered are the directions of symmetry axes of anisotropy. All noise levels yielded their reasonable estimates: The deviations of the optimum symmetry axes from the true axes were always less than 15°. Contrary to the orientation, the strength of anisotropy is more sensitive to noise in the data. The recovered strength yields a reasonable estimate of the true anisotropy strength for noise-free data and for data with noise levels I and II. Interestingly, the inversion of the noise-free data did not yield the true

Table 3. Synthetic Tests: Model and Inversion Constraints[a]

	A_{11}	A_{22}	A_{33}	A_{44}	A_{55}	A_{66}	A_{12}	A_{13}	A_{23}
True values	106	108	110	33	27	38	50	45	40
Limits in the Constrained Optimization									
Starting model	110	110	110	33	33	33	44	44	44
Lower limit	90	90	110	33	15	15	20	20	20
Upper limit	130	130	110	33	50	50	65	65	65

[a]Lower/upper limits define the intervals for sought optimum parameters; true values are parameters of synthetic anisotropy. Density-normalized elastic parameters are in km^2/s^2.

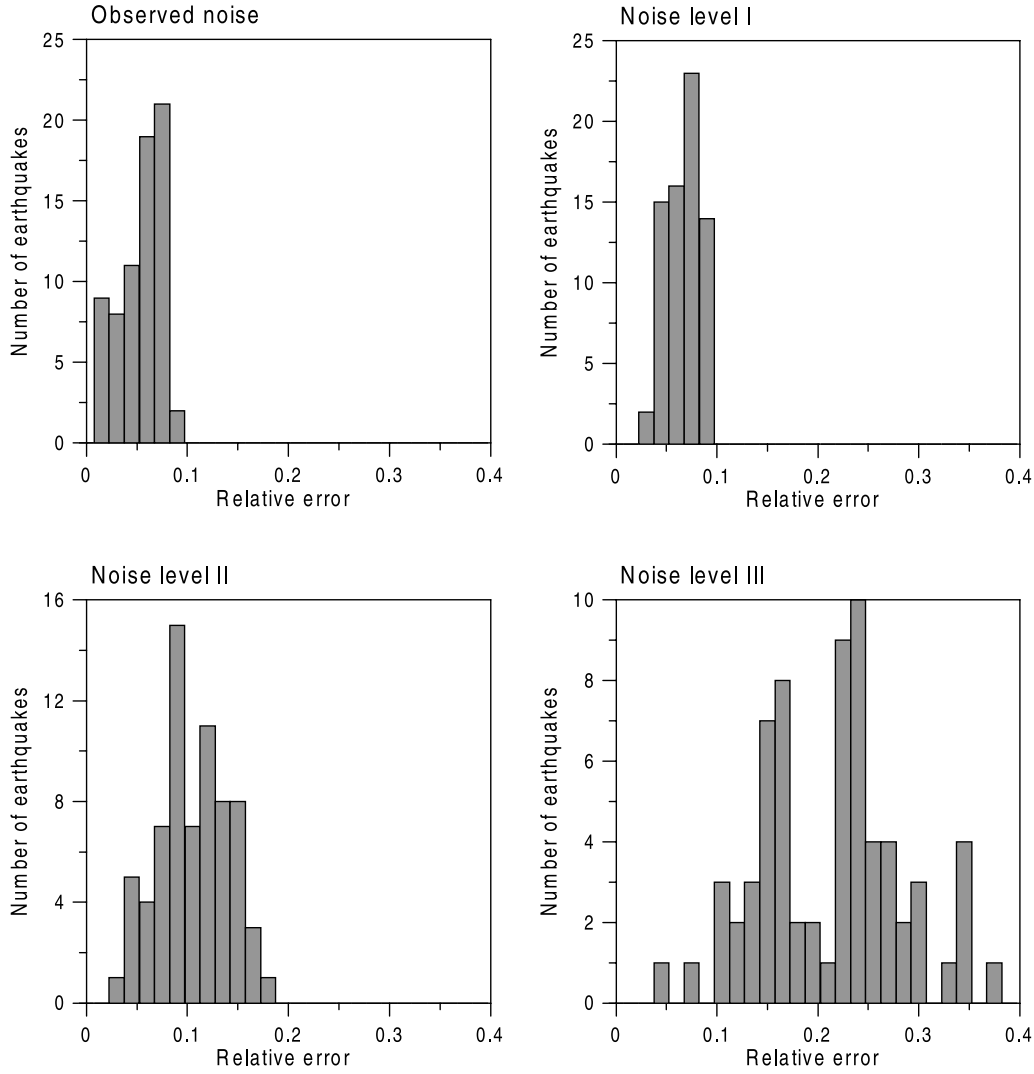

Figure 7. Synthetic and observed noise. The plots show histograms of relative errors of moment tensors observed in data set A and generated for synthetic tests.

anisotropy strength but slightly underestimated values. This is caused by the slightly misoriented anisotropy axes found by the grid search (the true anisotropy axes do not coincide with any grid node). Also, the inversion for noise level I yielded slightly underestimated values. However, the anisotropy strength is significantly overestimated for noise level III, indicating that the inversion becomes unstable. Hence the inversion for no noise or very small noise in the data tends to underestimate the anisotropy strength, but for higher noise levels the inversion becomes unstable, and the retrieved strength rapidly increases.

[23] Summarizing the synthetic tests, we can conclude that the inversion should be capable of yielding reliable estimates of anisotropy orientation and rough estimates of anisotropy strength in the Tonga subduction zone from the observed moment tensors. Since noise in the synthetic tests was simple and could not simulate actual properties of noise in the observed data (e.g., potential systematic errors in the moment tensors), the errors of retrieved values may be underestimated in the synthetic tests.

3.6. Inversion From Observed Data

[24] The inversion was performed analogously to synthetic tests. Parameters A_{33} and A_{44} were fixed in the inversion, even though it is difficult to estimate their values in the Earth, because isotropic velocity models yield spa-

Table 4. Synthetic Tests: Orientation and Strength of Anisotropy

Data Set	Axis 1 Azimuth/Dip, deg.	Axis 2 Azimuth/Dip, deg.	Axis 3 Azimuth/Dip, deg.	*P* Wave Anisotropy, %	*S*1 Wave Anisotropy, %	*S*2 Wave Anisotropy, %
True values	313/50	125/40	220/86	6.0	13.0	11.8
Noise free	310/50	130/40	220/90	6.1 ± 0.8	12.4 ± 1.3	10.6 ± 1.2
Noisy data I	320/50	130/40	220/84	6.0 ± 0.8	12.0 ± 0.9	9.6 ± 1.3
Noisy data II	310/51	130/40	220/90	5.3 ± 1.4	10.3 ± 1.3	12.9 ± 1.8
Noisy data III	320/60	120/36	225/81	9.7 ± 2.2	21.8 ± 4.5	15.6 ± 5.1

Table 5. Observed Data: Inversion Constraints and Optimum Density-Normalized Elastic Parameters[a]

	A_{11}	A_{22}	A_{33}	A_{44}	A_{55}	A_{66}	A_{12}	A_{13}	A_{23}
Limits in the Constrained Optimization									
Starting model	110	110	110	33	33	33	44	44	44
Lower limit	90	90	90	15	15	15	20	20	20
Upper limit	130	130	130	50	50	50	65	65	65
Dense Grid									
Optimum values	107.6	114.1	103.3	28.2	39.5	34.3	37.0	48.2	38.0

[a]Lower/upper limits define the intervals for sought density-normalized elastic parameters (in km^2/s^2).

tially averaged P and S velocities but not values of specific elastic parameters of the elasticity tensor. Therefore a series of inversions was performed with different values of A_{33} and A_{44}. For the found models the averaged P and S velocities were calculated and used as a criterion to select an optimum model. The optimum model was characterized by values of 110 and 33 km^2/s^2. These values were derived from the squares of the P and S velocities of model AK135 [*Kennett et al.*, 1995], averaged over the depth range 500–660 km and increased by 5% to reflect a high-velocity anomaly in the slab [*Zhou*, 1990a; *Zhao*, 2001]. I performed the inversions for data sets A–E. The values of the elastic parameters were sought within the intervals given in Table 5. The orientation of the symmetry axes was sought over a sphere in a grid with a step of 10°.

[25] The results are summarized in Tables 5 and 6. The orientations of the symmetry axes found are consistent for all data sets used. Figure 8 shows the misfit function evaluated for each direction of symmetry axis a_3 of orthorhombic anisotropy when inverting data set C. The misfit function is normalized so that it equals 1 for an isotropic medium. The best solutions lower the misfit function from 1 to 0.8; hence anisotropy is able to explain only a part of the non-DC components in the moment tensors. The function displays three distinct minima. The directions of the minima are mutually perpendicular and correspond to directions of the symmetry axes. Two symmetry axes lie within the slab; the third axis is close to the direction of the normal to the slab. The directions of the symmetry axes coincide with directions of the principal stresses (see Figure 9). Compared with the orientation, the estimates of strength of anisotropy are less consistent for the different data sets used. The strength is probably slightly underestimated for data set A but is overestimated for data sets D and E. This is confirmed by another inversion of data set A performed using a denser grid around the minimum of the misfit function found by previous inversions. The angles defining symmetry axis a_3 were limited to vary within the intervals (azimuth/dip) 320° ± 20°/50° ± 20° with step of 2°. The direction 320°/50° defines the minimum of the misfit function corresponding to the downdip motion of the slab. Since data set A consists of the most accurate moment tensors and the grid search is very dense, the estimates of anisotropy strength (see Table 6) and of elastic parameters (see Table 5) are probably most reliable.

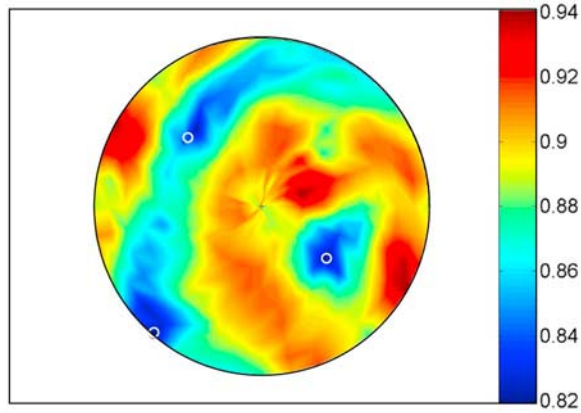

Figure 8. Inversion for orthorhombic anisotropy using moment tensors of data set C. The plot shows the misfit function for symmetry axes of orthorhombic anisotropy, normalized to the misfit for an isotropic medium. The misfit functions are displayed in the lower hemisphere equal-area projection. The optimum directions of the symmetry axes of anisotropy are marked by circles.

[26] In contrast to the absolute value of anisotropy strength, which is rather uncertain, the ratio of the S-to-P anisotropy strength is stable for all inversions. The anisotropy of S waves is always more pronounced, being about twice as high as the anisotropy of P waves. The ratio does not depend on values of the fixed averaged P and S wave velocities. Similarly, the spatial variation of the P, $S1$, and $S2$ velocities is stable and consistent for different data sets. The velocities of the resultant anisotropy vary within the following intervals (see Figure 10): 10.0 km/s < V_P < 10.8 km/s, 5.5 km/s < V_{S1} < 6.3 km/s, and 5.3 km/s < V_{S2} < 6.0 km/s. The average P, $S1$, and $S2$ velocities are 10.5, 6.0, and 5.6 km/s, respectively. The spatial variation of the P velocity has two distinct maxima: One is in a nearly vertical direction, and the other is nearly horizontal, being perpendicular to the trench. The $S1$ velocity has its maximum along the downdip compression and along the normal of the slab. The $S2$ velocity has a minimum along the downdip compression and also along the σ_3 axis. The maximum of the $S2$ velocity is broad and close to the normal of the slab.

Table 6. Observed Data: Orientation and Strength of Anisotropy

Data Set	Axis 1 Azimuth/Dip, deg.	Axis 2 Azimuth/Dip, deg.	Axis 3 Azimuth/Dip, deg.	P Wave Anisotropy, %	$S1$ Wave Anisotropy, %	$S2$ Wave Anisotropy, %
A	332/56	114/41	230/70	4.7 ± 1.4	10.4 ± 2.5	9.3 ± 1.7
B	320/53	121/40	227/80	7.3 ± 2.0	15.0 ± 3.0	14.1 ± 3.3
C	326/51	122/40	228/80	7.1 ± 2.1	13.7 ± 3.7	11.5 ± 3.3
D	313/51	130/40	220/84	8.7 ± 1.7	16.8 ± 3.3	14.0 ± 3.0
E	320/51	130/40	225/82	8.2 ± 2.0	16.3 ± 3.7	11.8 ± 3.2
Dense Grid						
A	320/54	121/38	223/81	7.3 ± 1.4	13.4 ± 2.5	12.6 ± 3.5

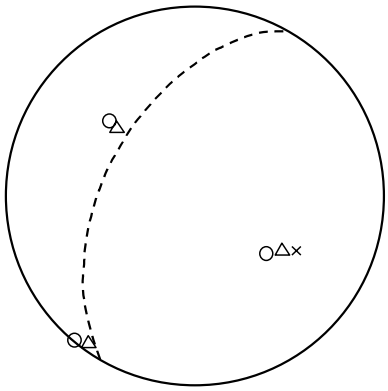

Figure 9. A comparison of slab, stress, and anisotropy orientations. The directions of the slab normal (cross), of the principal stress axes (triangles), and of the symmetry axes of anisotropy (circles) were calculated for moment tensors of data set C. Lower hemisphere equal-area projection is used. The dashed line shows the intersection of the slab with the hemisphere.

[27] The retrieved anisotropy can be used to predict the CLVD and ISO components caused by shear faulting in the anisotropic slab (Figure 11). The predicted values of the CLVD are asymmetric similarly to the observed ones: For data set A the mean value is −4.8%, and the mean of the absolute values is 8.8%. Although the observed and predicted values follow in average similar trends (see Figures 6 and 11), their coincidence for individual earthquakes is rather poor. The correlation between the predicted and observed CLVD is only 0.3. This confirms that anisotropy itself cannot fully explain the observed CLVD. The ISO component is significantly smaller than the CLVD. The mean value is only −1.2%, and the mean of the absolute values is 1.2%. The small predicted values of the ISO are of particular interest because they could explain why the ISO components have not been reliably detected yet [*Kawakatsu*, 1991, 1996; *Hara et al.*, 1995]. It should be emphasized that the predicted insignificant ISO components are not a consequence of the zero-trace moment tensors used in the inversion because the inversion only exploited the information on the CLVD.

4. Discussion

[28] The proposed inversion for anisotropy has the following advantages and limitations.

[29] 1. In contrast to the standard determination of anisotropy from travel times or from shear wave splitting, which yields an overall anisotropy averaged along a whole ray path, the proposed method gives a local value of anisotropy just in a focal area. Hence it should, in principle, be capable of retrieving the anisotropy of a focal area that is surrounded by a differently anisotropic or by an isotropic medium. The case when the surrounding medium is differently anisotropic is particularly complicated for standard methods because the effects of focal anisotropy can easily be masked by those of the surrounding medium. Of course, if the surrounding medium displays a remarkable anisotropy, the moment tensors must be determined using anisotropic Green functions.

[30] 2. The method is applicable under the following assumptions: Anisotropy must be uniform in the focal area; the earthquakes must occur on faults with varying orientations; and the earthquakes must be produced by shear faulting. If earthquakes are generated by tensile faulting [*Vavryčuk*, 2001], the method should be modified.

[31] 3. The accuracy of moment tensors must be very high because non-DC components, which are essential for this method, are very sensitive to errors in the moment tensors. This is a rather severe limitation because the

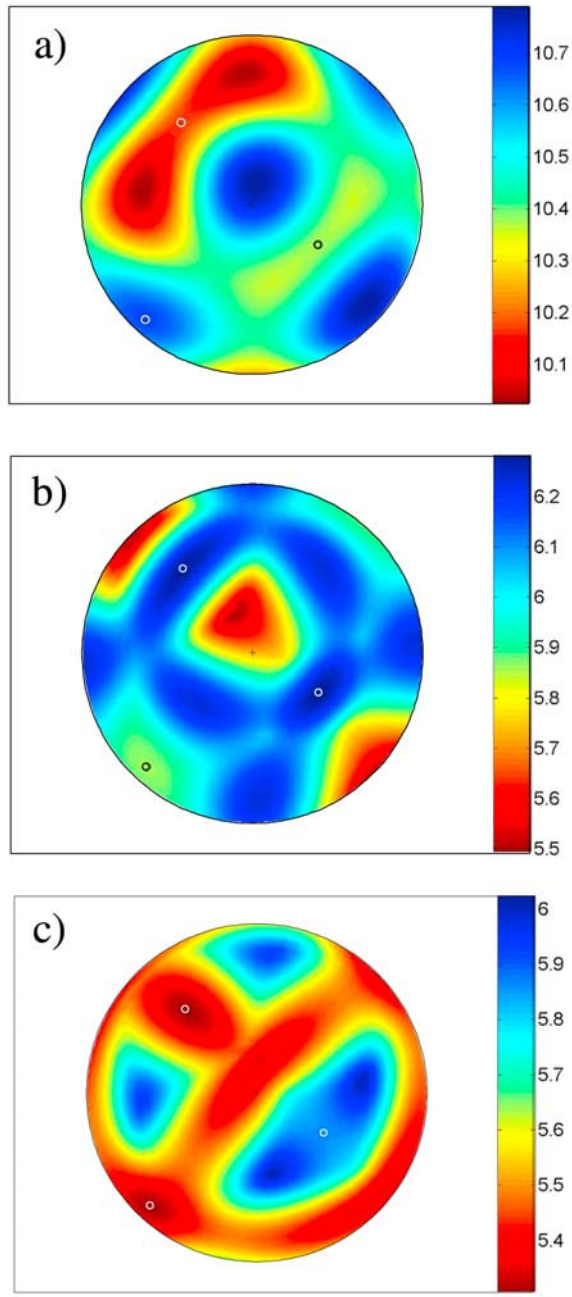

Figure 10. Spatial variation of the velocity predicted by the optimum anisotropy model for (a) *P*, (b) *S*1, and (c) *S*2 waves. Lower hemisphere equal-area projection is used. Directions of the symmetry axes are marked by circles. Velocities are in km/s.

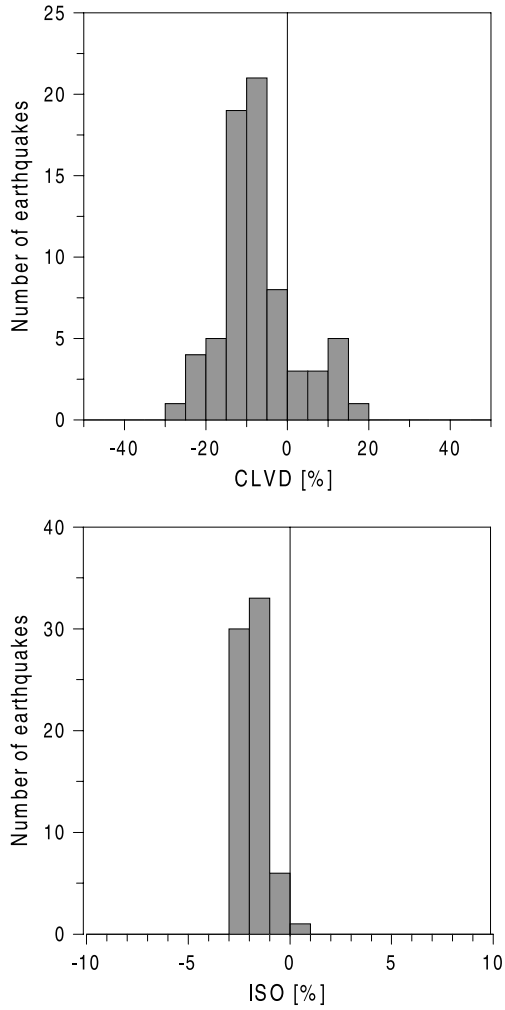

Figure 11. Histograms of (top) theoretical CLVD and (bottom) theoretical ISO components in the moment tensors of data set A predicted by the optimum anisotropy model (see Tables 5 and 6, dense grid).

non-DC components can easily be distorted by using inaccurate Green functions or foci locations in the moment tensor inversion.

[32] 4. The method is very robust. If a large set of high-quality moment tensors is available, the inversion can retrieve the orientation and strength of anisotropy even for low anisotropy symmetries as for orthorhombic symmetry.

[33] 5. The method cannot yield the complete elasticity tensor. Because of coupling between the slip, fault area, and elastic parameters and because of special geometry of faulting (shear faulting), two elastic parameters must always be fixed. Fortunately, the strength of anisotropy and the spatial variation of velocities are not very sensitive to the actual values of the parameters fixed. Of course, if the estimates are significantly biased from the correct values, the inversion can fail.

[34] 6. The method allows utilizing the moment tensors constrained to have zero trace, but using unconstrained moment tensors is advantageous. Assuming the zero trace of the moment tensor, the inversion for anisotropy is limited to inverting the CLVD components only. If full moment tensors are available, the method can invert for anisotropy using not only the CLVD but also the ISO components. Even the zero ISO components found, but not assumed, bring valuable information, which can be utilized in the inversion. Therefore reporting full moment tensors in global or regional moment tensor catalogs is highly desirable.

[35] The proposed inversion for anisotropy has been applied to moment tensors in the Tonga subduction zone. The results suggest that one of the causes generating non-DC components in the moment tensors of the deep earthquakes in the Tonga subduction zone is anisotropy of the slab. The other causes generating the non-DC components are probably mechanisms that changed during rupture and the errors produced by the moment tensor inversion due to unmodeled path effects. The presence of anisotropy in the slab is supported by the following observations.

[36] 1. The anisotropy found can explain an appreciable part of the CLVD components in the moment tensors.

[37] 2. In accordance with observations, the anisotropy generates no ISO components or very small ISO components.

[38] 3. The anisotropy is oriented consistently with stress in the slab. This is a reasonable and expected result [*Savage*, 1999], which manifests a success of the inversion. This success is conditioned by inverting highly accurate moment tensors. If less reliable data are used, the inversion fails.

[39] The orientation of the retrieved intra-slab anisotropy is defined by axes (azimuth/dip) $a_1 = 320°/54°$, $a_2 = 121°/38°$, and $a_3 = 223°/81°$. The errors in the azimuth and dip are about 5°. The first and second axes lie along the downdip motion of the slab and along the normal to the slab, respectively. The strength of the *P*, *S*1, and *S*2 anisotropy is of 7.3 ± 1.5%, 13.4 ± 2.5%, and 12.6 ± 3.5%, respectively. The errors of anisotropy strength are only rough estimates, which reflect random but not systematic errors in the moment tensors used in the inversion. For example, the systematic errors can be produced by using the isotropic Green functions in the moment tensor inversion or by confining moment tensors to have the zero trace. Therefore the true errors may be larger. In future studies a thorough analysis of the systematic errors in the CMT catalog and their influence on the anisotropy inversion will be necessary to achieve more reliable and more accurate estimates of retrieved anisotropy.

[40] Although the actual accuracy of the retrieved anisotropy strength is disputable, it is clear that the intra-slab anisotropy is remarkably higher than the estimates reported for the surrounding mantle. The *S* wave anisotropy in the mantle wedge is assumed to be varying, but its strength probably does not exceed 4% [*Ando et al.*, 1983; *Fischer and Wiens*, 1996]. The upper transition zone (410–520 km) is assumed to be weakly anisotropic with strength less than 0.5% [*Fouch and Fischer*, 1996; *Savage*, 1999]. The lower transition zone (520–660 km) and the lower mantle are reported to be nearly isotropic [*Fouch and Fischer*, 1996; *Fischer et al.*, 1998]. Anisotropy may also exist near the 660 km discontinuity with strength up to 3% [*Wookey et al.*, 2002]. Compared with these results, the retrieved intra-slab anisotropy is strong and indicates anomalous properties of the subducting slab. It points to the presence of highly anisotropic minerals with a high degree of alignment in the slab. Since the orientation of anisotropy coincides with the orientation of stress in the slab, the stress is probably a key

factor in formation of anisotropy. Stress may cause alignment of anisotropic minerals that produces an overall anisotropy of the slab.

[41] The proposed inversion can find other attractive applications. Collecting a sufficiently high number of carefully determined moment tensors, we can probe anisotropy in various slabs or explore variations of anisotropy along a slab. This could help us to understand better the changes in the composition and structure of a slab owing to the 220, 410, and 520 km discontinuities.

[42] **Acknowledgments.** The author thanks Vladislav Babuška, Cliff Frohlich, Joan Gomberg, Axel Plešinger, Ivan Pšenčík, Jan Šílený, and an anonymous reviewer for their comments. The work was supported by the Grant Agency of the Academy of Sciences of the Czech Republic, grant A3012309, and by the Grant Agency of the Czech Republic, grant 205/02/0383.

References

Aki, K., and P. G. Richards (2002), *Quantitative Seismology*, Univ. Sci., Sausalito, Calif.

Anderson, D. L. (1987), Thermally induced phase changes, lateral heterogeneity of the mantle, continental roots and deep slab anomalies, *J. Geophys. Res.*, *92*, 13,968–13,980.

Ando, M., W. Ishikawa, and F. Yamazaki (1983), Shear waves polarization anisotropy in the upper mantle beneath Honshu, Japan, *J. Geophys. Res.*, *88*, 5850–5864.

Babuška, V., and M. Cara (1991), *Seismic Anisotropy in the Earth*, Kluwer Acad., Norwell, Mass.

Branch, M. A., and A. Grace (1996), *MATLAB Optimization Toolbox*, The MathWorks, Natick, Mass.

Deal, M. M., G. Nolet, and R. D. van der Hilst (1999), Slab temperature and thickness from seismic tomography: 1. Method and application to Tonga, *J. Geophys. Res.*, *104*, 28,789–28,802.

DeMets, C., R. G. Gordon, D. F. Argus, and S. Stein (1990), Current plate motions, *Geophys. J. Int.*, *101*, 425–478.

Dziewonski, A. M., G. Ekström, and N. N. Maternovskaya (2001), Centroid moment tensor solutions for July–September 2000, *Phys. Earth Planet. Inter.*, *124*, 9–23.

Dziewonski, A. M., G. Ekström, and N. N. Maternovskaya (2003), Centroid moment tensor solutions for October–December 2000, *Phys. Earth Planet. Inter.*, *136*, 145–164.

Estabrook, C. H. (1999), Body wave inversion of the 1970 and 1963 South American large deep-focus earthquakes, *J. Geophys. Res.*, *104*, 28,751–28,767.

Feignier, B., and R. P. Young (1992), Moment tensor inversion of induced microseismic events: Evidence of non-shear failures in the $-4 < M < -2$ moment magnitude range, *Geophys. Res. Lett.*, *19*, 1503–1506.

Fischer, K. M., and D. A. Wiens (1996), The depth distribution of mantle anisotropy beneath the Tonga subduction zone, *Earth Planet. Sci. Lett.*, *142*, 253–260.

Fischer, K. M., M. J. Fouch, D. A. Wiens, and M. S. Boettcher (1998), Anisotropy and flow in Pacific subduction zone back-arcs, *Pure Appl. Geophys.*, *151*, 463–475.

Fouch, M. J., and K. M. Fischer (1996), Mantle anisotropy beneath northwest Pacific subduction zones, *J. Geophys. Res.*, *101*, 15,987–16,002.

Frohlich, C. (1989), The nature of deep-focus earthquakes, *Annu. Rev. Earth Planet. Sci.*, *17*, 227–254.

Frohlich, C. (1994), Earthquakes with non-double-couple mechanisms, *Science*, *264*, 804–809.

Frohlich, C., and S. D. Davis (1999), How well constrained are well-constrained *T*, *B*, and *P* axes in moment tensor catalogs?, *J. Geophys. Res.*, *104*, 4901–4910.

Fukao, Y. (1984), Evidence from core-reflected shear waves for anisotropy in the Earth's mantle, *Nature*, *309*, 695–698.

Gephart, J. W. (1990), Stress and the direction of the slip on fault planes, *Tectonics*, *9*, 845–858.

Gephart, J. W., and D. W. Forsyth (1984), An improved method for determining the regional stress tensor using earthquake focal mechanism data: Application to the San Fernando earthquake sequence, *J. Geophys. Res.*, *89*, 9305–9320.

Giardini, D. (1992), Space-time distribution of deep seismic deformation in Tonga, *Phys. Earth Planet. Inter.*, *74*, 75–88.

Giardini, D., and J. H. Woodhouse (1984), Deep seismicity and modes of deformation in Tonga subduction zone, *Nature*, *307*, 505–509.

Gill, P. E., W. Murray, and M. H. Wright (1991), *Numerical Linear Algebra and Optimization*, vol. 1, Addison-Wesley-Longman, Reading, Mass.

Gripp, A. E., and R. G. Gordon (1990), Current plate velocities relative to the hotspots incorporating the NUVEL-1 global plate motion model, *Geophys. Res. Lett.*, *17*, 1109–1112.

Guest, A., G. Schubert, and C. Gable (2004), Stresses along the metastable wedge of olivine in a subducting slab: Possible explanation for the Tonga double seismic layer, *Phys. Earth Planet. Inter.*, *141*, 253–267.

Hamburger, M. W., and B. L. Isacks (1987), Deep earthquakes in the southwest Pacific: A tectonic interpretation, *J. Geophys. Res.*, *92*, 13,841–13,854.

Hara, T., K. Kuge, and H. Kawakatsu (1995), Determination of the isotropic component of the 1994 Bolivia deep earthquake, *Geophys. Res. Lett.*, *22*, 2265–2268.

Hasegawa, H. S., and H. Kanamori (1987), Source mechanism of the magnitude 7.2 Grand Banks earthquake of November 1929: Double couple or submarine landslide?, *Bull. Seismol. Soc. Am.*, *77*, 1984–2004.

Helffrich, G. R. (1997), How good are routinely determined focal mechanisms? Empirical statistics based on a comparison of Harvard, USGS and ERI moment tensors, *Geophys. J. Int.*, *131*, 741–750.

Hiramatsu, Y., M. Ando, and Y. Ishikawa (1997), ScS wave splitting of deep earthquakes around Japan, *Geophys. J. Int.*, *128*, 409–424.

Isacks, B., and P. Molnar (1971), Distribution of stresses in the descending lithosphere from a global survey of focal-mechanism solutions of mantle earthquakes, *Rev. Geophys.*, *9*, 103–174.

Jost, M. L., and R. B. Hermann (1989), A student's guide to and review of moment tensors, *Seismol. Res. Lett.*, *60*, 37–57.

Julian, B. R., A. D. Miller, and G. R. Foulger (1998), Non-double-couple earthquakes: 1. Theory, *Rev. Geophys.*, *36*, 525–549.

Kagan, Y. Y. (2003), Accuracy of modern global earthquake catalogs, *Phys. Earth Planet. Inter.*, *135*, 173–209.

Karato, S., M. R. Riedel, and D. A. Yuen (2001), Rheological structure and deformation of subducted slabs in the mantle transition zone: Implications for mantle circulation and deep earthquakes, *Phys. Earth Planet. Inter.*, *127*, 83–108.

Kawakatsu, H. (1991), Insignificant isotropic component in the moment tensor of deep earthquakes, *Nature*, *351*, 50–53.

Kawakatsu, H. (1995), Automated near-realtime CMT inversion, *Geophys. Res. Lett.*, *22*, 2569–2572.

Kawakatsu, H. (1996), Observability of the isotropic component of a moment tensor, *Geophys. J. Int.*, *126*, 525–544.

Kawasaki, I., and T. Tanimoto (1981), Radiation patterns of body waves due to the seismic dislocation occurring in an anisotropic source medium, *Bull. Seismol. Soc. Am.*, *71*, 37–50.

Kendall, J.-M., and C. Thomson (1993), Seismic modelling of subduction zones with inhomogeneity and anisotropy: I. Teleseismic *P*-wavefront tracking, *Geophys. J. Int.*, *112*, 39–66.

Kennett, B. L. N., E. R. Engdahl, and R. Buland (1995), Constraints on seismic velocities in the Earth from travel times, *Geophys. Int, J.*, *122*, 108–124.

Knopoff, L., and M. J. Randall (1970), The compensated linear vector dipole: A possible mechanism for deep earthquakes, *J. Geophys. Res.*, *75*, 4957–4963.

Koper, K. D., D. A. Wiens, L. Dorman, J. Hildebrand, and S. Webb (1999), Constraints on the origin of slab and mantle wedge anomalies in Tonga from the ratio of *S* to *P* velocities, *J. Geophys. Res.*, *104*, 15,089–15,104.

Kuge, K., and H. Kawakatsu (1992), Deep and intermediate depth non-double couple earthquakes: Interpretation of moment tensor inversions using various passbands of very broad-band seismic waves, *Geophys. J. Int.*, *111*, 589–606.

Kuge, K., and H. Kawakatsu (1993), Significance of non-double-couple components of deep and intermediate-depth earthquakes: Implications from moment tensor inversions of long-period waves, *Phys. Earth Planet. Inter.*, *75*, 243–266.

Kuge, K., and T. Lay (1994), Data-dependent non-double-couple components of shallow earthquake source mechanisms: Effects of waveform inversion instability, *Geophys. Res. Lett.*, *21*, 9–12.

Lund, B., and R. Slunga (1999), Stress tensor inversion using detailed microearthquake information and stability constraints: Application to Ölfus in southwest Iceland, *J. Geophys. Res.*, *104*, 14,947–14,964.

Mainprice, D., G. Barruol, and W. Ben Ismail (2000), The seismic anisotropy of the Earth's mantle: From single crystal to polycrystal, in *Earth's Deep Interior: Mineral Physics and Tomography From the Atomic to the Global Scale*, *Geophys. Monogr. Ser.*, vol. 117, edited by S. Karato et al., pp. 237–264, AGU, Washington, D. C.

McNamara, A. K., P. E. van Keken, and S. Karato (2002), Development of anisotropic structure in the Earth's lower mantle by solid-state convection, *Nature*, *416*, 310–314.

Michael, A. J. (1987), Use of focal mechanisms to determine stress: A control study, *J. Geophys. Res.*, *92*, 357–368.

Miller, A. D., G. R. Foulger, and B. R. Julian (1998), Non-double-couple earthquakes: 2. Observations, *Rev. Geophys.*, *36*, 551–568.

Mori, J., and C. McKee (1987), Outward-dipping ring-fault structure at Rabaul caldera as shown by earthquake locations, *Science*, *235*, 193–195.

Musgrave, M. J. P. (1970), *Crystal Acoustics*, Holden-Day, Boca Raton, Fla.

Northard, S., D. McKenzie, J. Haines, and J. Jackson (1996), Gaussian curvature and the relationship between the shape and the deformation of the Tonga slab, *Geophys. J. Int.*, *127*, 311–327.

Powell, M. J. D. (1978), A fast algorithm for nonlinearly constrained optimization calculations, in *Numerical Analysis*, *Lect. Notes Math.*, vol. 630, edited by G. A. Watson, pp. 144–157, Springer-Verlag, New York.

Rudajev, V., and J. Šílený (1985), Seismic events with non-shear components: II. Rockbursts with implosive source component, *Pure Appl. Geophys.*, *123*, 17–25.

Savage, M. K. (1999), Seismic anisotropy and mantle deformation: What have we learned from shear wave splitting?, *Rev. Geophys.*, *37*, 65–106.

Šílený, J., and V. Vavryčuk (2000), Approximate retrieval of the point source in anisotropic media: Numerical modelling by indirect parametrization of the source, *Geophys. J. Int.*, *143*, 700–708.

Šílený, J., and V. Vavryčuk (2002), Can unbiased source be retrieved from anisotropic waveforms by using an isotropic model of the medium?, *Tectonophysics*, *356*, 125–138.

Sipkin, S. A. (1986), Interpretation of non-double-couple earthquake mechanisms derived from moment tensor inversion, *J. Geophys. Res.*, *91*, 531–547.

Sipkin, S. A., C. G. Bufe, and M. D. Zirbes (2002), Moment-tensor solutions estimated using optimal filter theory: Global seismicity, 2000, *Phys. Earth Planet. Inter.*, *130*, 129–142.

Tibi, R., G. Bock, and D. A. Wiens (2003), Source characteristics of large deep earthquakes: Constraint on the faulting mechanism at great depths, *J. Geophys. Res.*, *108*(B2), 2091, doi:10.1029/2002JB001948.

Vavryčuk, V. (2001), Inversion for parameters of tensile earthquakes, *J. Geophys. Res.*, *106*, 16,339–16,355.

Vavryčuk, V. (2002), Non-double-couple earthquakes of 1997 January in West Bohemia, Czech Republic: Evidence of tensile faulting, *Geophys. J. Int.*, *149*, 364–373.

Wookey, J., J.-M. Kendall, and G. Barruol (2002), Mid-mantle deformation inferred from seismic anisotropy, *Nature*, *415*, 777–780.

Zhao, D. (2001), Seismological structure of subduction zones and its implications for arc magmatism and dynamics, *Phys. Earth Planet. Inter.*, *127*, 197–214.

Zhou, H. (1990a), Mapping of *P*-wave slab anomalies beneath the Tonga, Kermadec and New Hebrides arcs, *Phys. Earth Planet. Inter.*, *61*, 199–229.

Zhou, H. (1990b), Observations on earthquake stress axes and seismic morphology of deep slabs, *Geophys. J. Int.*, *103*, 377–401.

V. Vavryčuk, Geophysical Institute, Academy of Sciences of the Czech Republic, Bocni II/1401, 141 31 Praha 4, Czech Republic. (vv@ig.cas.cz)